Molecular Basis of the Antioxidant Capability of Glutathione Unraveled via Aerosol VUV Photoelectron Spectroscopy

Po-Chiao Chang, Youqing Yu, Zhong-Hang Wu, Ping-Cheng Lin, Wei-Ren Chen,

Chien-Cheng Su, Meng-Sin Chen, Yu-Lin Li, Tzu-Ping Huang, Yin-Yu Lee

and Chia C. Wang*

S.1. Size distribution of GSH aqueous aerosols at varying pH

A fraction of GSH aqueous aerosols generated from the atomizer was directed to the scanning mobility particle sizer (SMPS, Model 3936, TSI Inc.), from which the size distribution and the number density of GSH aqueous aerosols at four chosen pH conditions were measured before entering the AADL system.
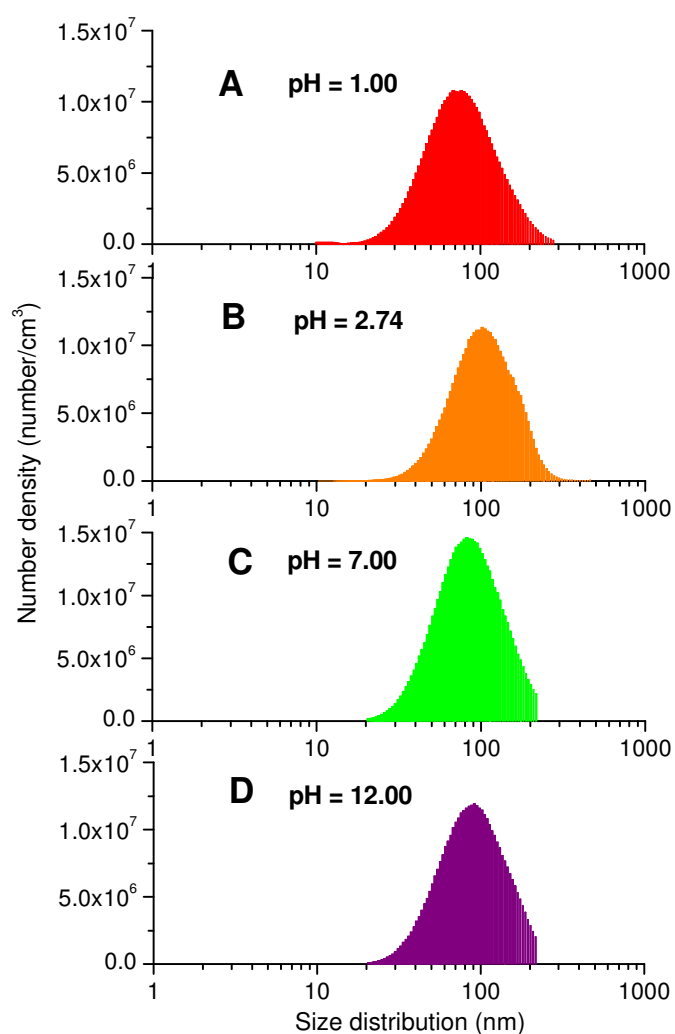

Figure S1 Size distribution of GSH aqueous aerosols at the four chosen pH conditions.

A. pH =1.00, B. pH = 2.74, C. pH = 7.00 and D. pH = 12.00.

S.2. Relative percentages of different GSH species at varying pH condition

The relative percentages of the seven possible GSH species (structures A to G illustrated in Scheme 1) at pH = 1.00, 2.74, 7.00, 9.00 and 12.00 are listed in Table S1, calculated based on the microscopic ionization constants of GSH reported by Rabenstein.[1]

Table S1. Percentages (%) of the seven GSH species at five representative pH conditions.

	A	B	C	D	E	F	G
pH	GSH^+	GSH (Glu_COO⁻)	GSH (Gly_COO⁻)	GSH^-	GSH^{2-} (S⁻)	GSH^{2-} (NH₂)	GSH^{3-}
1.00	91.81	7.46	0.70	3.26×10^{-2}	3.83×10^{-10}	2.41×10^{-10}	2.01×10^{-18}
2.74	14.38	64.22	5.99	15.41	9.95×10^{-6}	6.28×10^{-6}	2.87×10^{-12}
7.00	2.76×10^{-7}	2.25×10^{-2}	2.10×10^{-3}	98.09	1.15	0.73	6.05×10^{-3}
9.00	7.98×10^{-12}	6.48×10^{-5}	6.05×10^{-6}	28.31	33.26	20.98	17.45
12.00	4.56×10^{-23}	3.70×10^{-13}	3.46×10^{-14}	1.62×10^{-4}	0.19	0.12	99.69

Note that even though GSH^{2-} showed the highest fraction at pH = 9.0 (Figure 5D), two other GSH charge forms, including GSH^- and GSH^{3-} also account for non-negligible proportions at this pH (see also Figure 5D at pH = 9). Therefore, while the VUV photoelectron spectra of GSH have also been measured at pH = 9.00, the photoelectron spectra cannot represent a single major species due to the compositional complexity at this pH.

S.3. The nature of aqueous aerosols

The nature of aqueous aerosols can be tackled from several aspects, which indicate that the aqueous aerosols remain as supercooled liquids at the point of photoionization. First, one may compare the B.E. of $1b_1$ band of condensed water for aqueous aerosols directly with the previously reported B.E. values of liquid water and ice water. The B.E. for $1b_1$ band of liquid water has been characterized via the liquid microjet photoemission spectroscopy by several research groups with the reported B.E. ranging between 10.92 eV and 11.31 eV.[2-5] As addressed by Winter *et al*,[3] the B.E. of water ice is higher than the liquid water. The B.E. of the $1b_1$ band of water ice was reported to be between 12.3 eV and 11.8 eV.[6,7] In comparison, the B.E. of the condensed water is found to be situated at 10.83 ± 0.05 eV for the pure water aerosols,[8] and at around 11 eV for the solute-containing aqueous aerosols.[8] Both types of condensed water features in the aqueous aerosols match the B.E. value for the liquid water, indicating that aqueous aerosols appear to remain in the liquid phase.

From the second aspect, the aqueous aerosols are subjected to evaporative cooling before arriving at the photoionization region. The evaporation of water droplets has been considered previously in the microjet experiments.[9,10] According to the kinetic theory of evaporation, the evaporation rate can be described by the Hertz-Knudsen equation,

$$\frac{1}{A}\frac{dN}{dt} = J_{e,obs} = \gamma_e J_{e,max} = \frac{\gamma_e P_o}{\sqrt{2\pi m k_B T}} \qquad \text{(Equation 1)}$$

where $A = 4\pi r^2$ denotes the surface area of the aqueous aerosol; N denotes the number of gas molecules evaporated from the aqueous droplet; $J_{e,obs}$ denotes the observed evaporation rate; $J_{e,max}$ denotes the theoretical maximum evaporation rate; γ_e denotes the evaporation coefficient and P_o denotes the equilibrium vapor pressure.[10] The γ_e value for liquid water has been determined to be 0.62 ± 0.09 by Smith *et al*.[10] The size evolutions of water droplets of various diameters

ranging between 15.5 μm to 100 nm are thus estimated, expressed in terms of the ratio of diameters of water droplets before (d_o) and after evaporation (d) (Figure S2) as a function of flight time after exiting the AADL. The droplets of μm, which are relevant to the droplets produced in the microjet technique are also shown here to compare the evaporation of water droplets of varying size regimes.
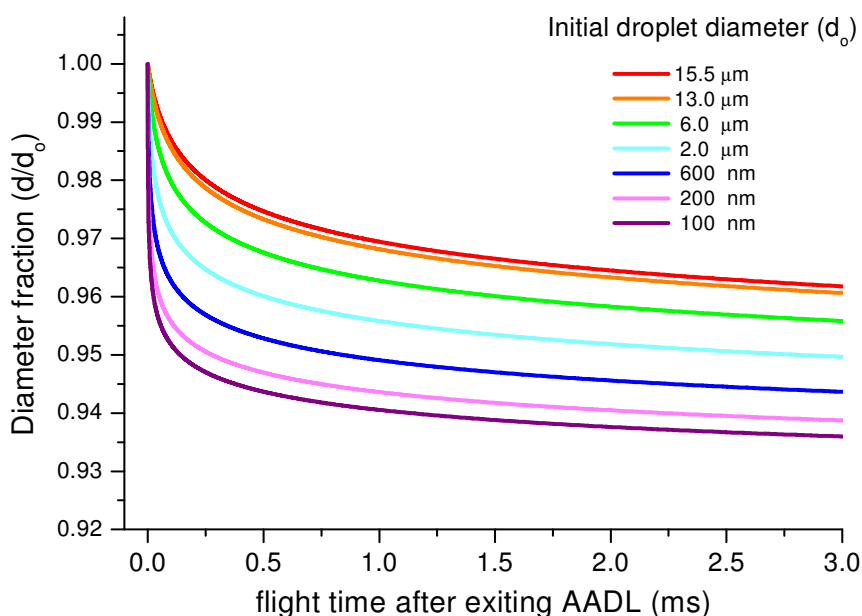

Figure S2. Size evolution of water droplets of varying initial diameters as a result of solvent evaporation.

For a water droplet with an initial diameter of ~ 100 nm, which is relevant to the aerosol size regime of this work, the size decreases abruptly to ~ 96 % of its original size within the first 30 μs after exiting the AADL. In the present experimental setup, the aqueous aerosols of an initial average diameter of 100 nm are expected to reach the photoionization region after a flight time of 2 ms after exiting the AADL with a beam speed of 145 m/s, as predicted from the

Aerodynamic Lens Calculator.[11] Accordingly, the aqueous aerosols of an initial average diameter of ~ 100 nm are expected to decrease to ~ 94 nm at the point of photoionization.

The temperature change of the aqueous aerosols accompanying with solvent evaporation can be expressed as:

$$\frac{dT}{dt} = -\gamma_e J_{e,max} A \frac{\Delta H_{vap}}{C_p M_d} \qquad \text{(Equation 2)}$$

where ΔH_{vap} (J/mol) is the enthalpy of evaporation; C_p (J/mol K) is the constant pressure heat capacity; $M_d = \frac{4}{3}\pi(r_0^3 - r_1^3)\rho_1$ represents the mass of the spherical shell with the width of $(r_0 - r_1)$ and the density of ρ_1.[10] By combining Eq. (1) and Eq. (2), the change of temperature of water droplets can be rewritten as:

$$\frac{dT}{dt} = -\frac{\gamma_e P_o}{\sqrt{2\pi m k_B T}} \cdot \frac{\Delta H_{vap}}{C_p} \cdot \frac{3r_o^2}{(r_0^3 - r_1^3)\rho_1} \qquad \text{(Equation 3)}$$

The Arden Buck equation is used to express the equilibrium vapor pressure P_o as a function of temperature.[12,13] The Kelvin effect of nanodroplet on the vapor pressure has also been considered; however, for the size regime of aqueous aerosols studied here, the curvature effect on the equilibrium vapor pressure is only moderate (~2 %). For the present experimental conditions, the aerosol temperature has been estimated to be ~193 K at the point of photoionization, implying that the aqueous aerosols are likely in a deeply supercooled liquid status.[9,10,14] While the glassy state of water may exist in nature, which once formed may retain the liquid-like, disordered structural arrangement while mechanically behaving like a solid, however, the glass transition temperature of water has been reported to be at 136 K,[15,16] which

appears too low for the aqueous aerosols in the present study to reach. Therefore the liquid nature of aqueous aerosols at the point of photoionization can be justified.

S.4. VUV photoelectron spectra of GSH aqueous aerosols at varying pH – an extended view

An extended view of the photoelectron spectra of GSH at pH = 1.00, 2.74, 7.00 and 12.00 are shown in Figure S3, where the photoelectron spectral feature of condensed water and partially the gas phase water are revealed. Resided between the binding energy (B.E.) of 12.6 and 13.5 eV are the ultrafine vibrational structures of the $1b_1$ band of gas phase water molecules. Though the main spectral feature of GSH demonstrates an explicit pH-dependent behavior, the B.E. for the condensed water remains unaltered at around 11 eV.

From Figure S3, the intensity of the condensed water feature at around 11 eV appears to vary with pH conditions of the aqueous aerosols. As discussed in the above section, the aqueous aerosols are not dried but remain in the liquid phase. Therefore, one possibility that may lead to such intensity reduction for the condensed water may be attributed to the post-ionization effect. While the GSH aqueous aerosols are generated with constant output liquid feed atomizer under the same conditions, the average size of GSH aqueous aerosols at pH = 2.74 appears to be larger than GSH aqueous aerosols prepared at other pH conditions (see Figure S1A to D for the size distribution of GSH aqueous aerosols at the four chosen pH conditions). Because the outgoing photoelectrons must escape the aerosol droplet to be detected, some electrons may undergo inelastic scattering with other molecules within the aerosol droplet and lose kinetic energy before escaping the aqueous droplets. Therefore, the relatively weaker intensity of condensed water feature at ~ 11 eV may indicate that relatively more photoelectrons undergo inelastic

scattering in the larger aerosols at pH = 2.74 before eventually escaping the droplet. The photoelectrons suffered from inelastically scattering should then contribute to the characteristic secondary photoelectron feature (not shown in the presented photoelectron spectra).
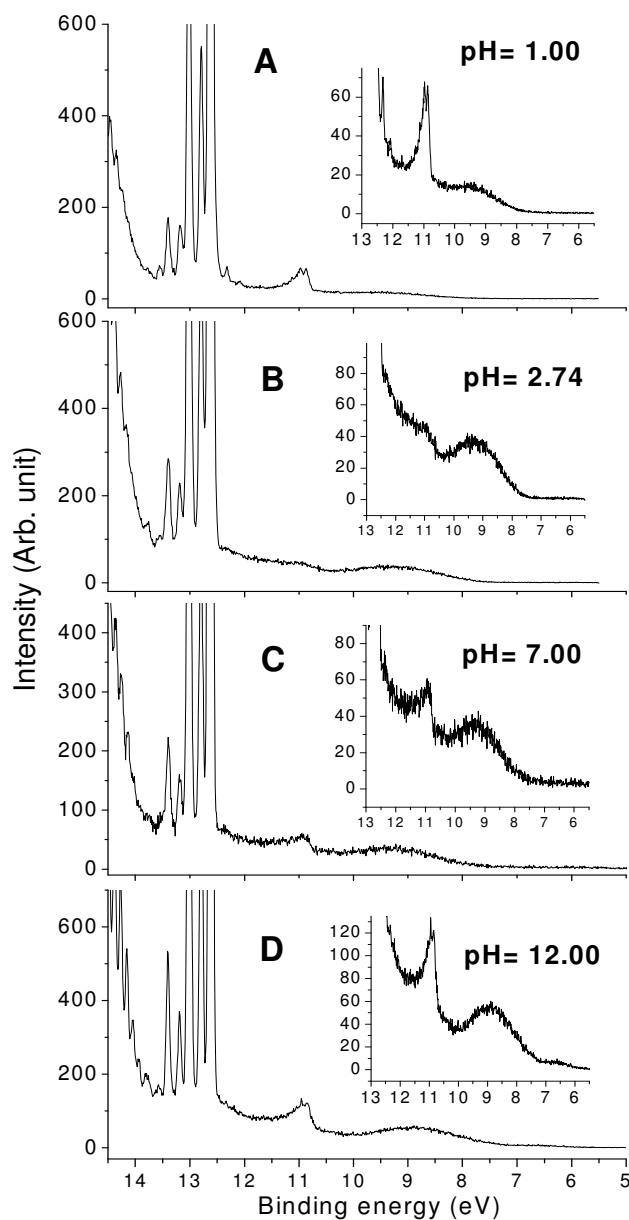

Figure S3 Extended views of the experimental VUV photoelectron spectra of GSH aqueous aerosols at: A. pH =1.00, B. pH = 2.74, C. pH = 7.00 and D. pH = 12.00.

The electron attenuation length (EAL) and inelastic mean free path (IMFP) of photoelectrons as a function of electron kinetic energy (eKE) from aqueous droplets and from aerosol particles has been an issue of concern and has been investigated by several researchers.[17-20] Suzuki *et al* experimentally estimated the EAL of electrons in liquid water with the eKE ranging between 10 and 600 eV,[19] while Signorell *et al* recently studied both the EAL and IMFP for electrons with low eKE (1-3 eV) in water aerosol droplets. In the present study, as the condensed water feature has an eKE value of ~ 13 eV (at a photon energy of 25 eV), the EAL is estimated to be at the order of sub nm.[19] Nevertheless, in addition to the effects of aerosol size and eKE on the EAL and IMFP in the aqueous aerosols, it will be of interest for one to interrogate the possible effects of chemical environment within the aerosol, such as the presence of charged ion species in affecting the escaping trajectory of ejecting photoelectrons.

S.5. VUV photoelectron spectra of Gly aqueous aerosols at varying pH

Glycine (Gly), the simplest and most well-studied α-amino acid has been the prototype molecule to study the general properties of amino acids. Although the valence electronic properties of Gly in the aqueous solution phase remain unavailable, the electronic structures of Gly have been studied under different phases and ionization sources by several authors. The gas phase valence electron structures of Gly have been reported via He(I)/He(II) photoemission spectra.[21-23] Plekan *et al*[24] investigated both the valence and core level photoelectron spectra of Gly in the gas phase, using the synchrotron-based VUV and soft X-ray radiation as the ionization sources. The core electronic structures of Gly in the solid state have also been studied by Gordon *et al*[25] and Zubavichus *et al*[26,27] using X-ray absorption spectra. However, the

structural information obtained from the gas phase studies is restricted to the neutral Gly molecule, and the solid state studies can only provide information regarding Gly in the zwitterionic form. As for Gly in the solution phase, only the core-level electronic properties were studied up to date. Gråsjö et al[28] studied the core-level oxygen and nitrogen K photoemission spectra of Gly in the solution by resonantly exciting oxygen and nitrogen sites, showing the dramatic influence of protonation status on the local core electronic structure of Gly in the solution. Ottosson et al[29] further utilized the X-ray microjet photoemission spectroscopy to measure the core-level nitrogen and carbon 1s binding energies of solvated Gly and discussed in details the origins underlying the observed core-level chemical shifts of an aqueous solute in its various possible protonation states. The valence electronic properties of Gly in the dehydrated nanoparticle phase were also interrogated by Wilson et al[30] by the synchrotron-based VUV velocity-mapping photoelectron imaging technique, from which the ionization energies and molecular polarizabilities of dehydrated Gly nanoparticles were reported.

Despite these extensive studies on the electronic properties of Gly, the valence electronic structures of Gly in the solution phase and its possible evolution remain unavailable. With the goals to obtain the valence electronic properties of Gly in the solution phase and to access the possible contribution of Gly to the electronic characters of GSH, here we measure the valence electronic properties of solvated Gly and its pH dependence for the first time in the form of aqueous aerosols.

With two possible protonation/deprotonation sites, Gly may exist in three different forms at varying pH conditions, including the protonated Gly^+, zwitterionic Gly and deprotonated Gly^-. Three representative pH conditions are specifically chosen for the photoelectron spectroscopic measurements of Gly based on the pKa values of Gly, such that Gly of a particular charged

status can be measured. The VUV photoelectron spectra of Gly aqueous aerosols at the three pH conditions, including pH = 1.00 (Figure S4A), 6.22 (Figure S4B), and 12.00 (Figure S4C) are measured, with each pH condition representing a dominating Gly species. At pH = 1.00 (Figure S3A), Gly exists primarily (~ 96%) as the protonated Gly^+ cation. The observed photoelectron spectrum shows a significant broad spectral feature centering at 9.70 ± 0.05 eV and a minor feature at around 11 eV. The broad feature centering at 9.70 eV can be attributed to the non-bonding electron on the oxygen atom (denoted as Gly n_O), while the minor feature at 11 eV is originated from the condensed water. To extract more insights, the observed photoelectron spectra of Gly is de-convoluted into several spectral components, including Gly n_O, (violet curves in Figure S4), the condensed water (cyan curves in Figure S4) and the gaseous water (gray curves in Figure S4). The accumulative curves are also shown (pink curves in Figure S4). At pH = 6.22 (Figure S4B), the Gly zwitterion becomes the dominant form (~99.9 %). Compared to the Gly photoelectron spectrum at pH =1.00, the B.E. of Gly n_O shifts from 9.70 to 9.29 ± 0.05 eV, corresponding to a B.E. reduction of 0.41 ± 0.05 eV. When the pH value is increased to 12.00 (Figure S4C), the main Gly feature is evidently further downshifted and broadened, while the position of the condensed water remains relatively unchanged at around 11 eV.

From the previous soft X-ray emission (SXE) spectroscopic study of Gly by Gråsjö et al[28], the local environments of the amine and carboxyl group were selectively probed by excitation via either oxygen or nitrogen K edges. The ionization energies of gas phase Gly n_N and Gly n_O were thus determined to be 10.00 eV and 11.20 eV respectively, and the highest occupied molecular orbital (HOMO) for the gas phase Gly was reported to be the non-bonding electron on nitrogen, Gly n_N. Therefore, the broadened Gly feature observed at pH=12.00 should be

contributed from two spectral components, including the Gly n_O feature and the Gly n_N feature which becomes available for ionization when the amine group is deprotonated.
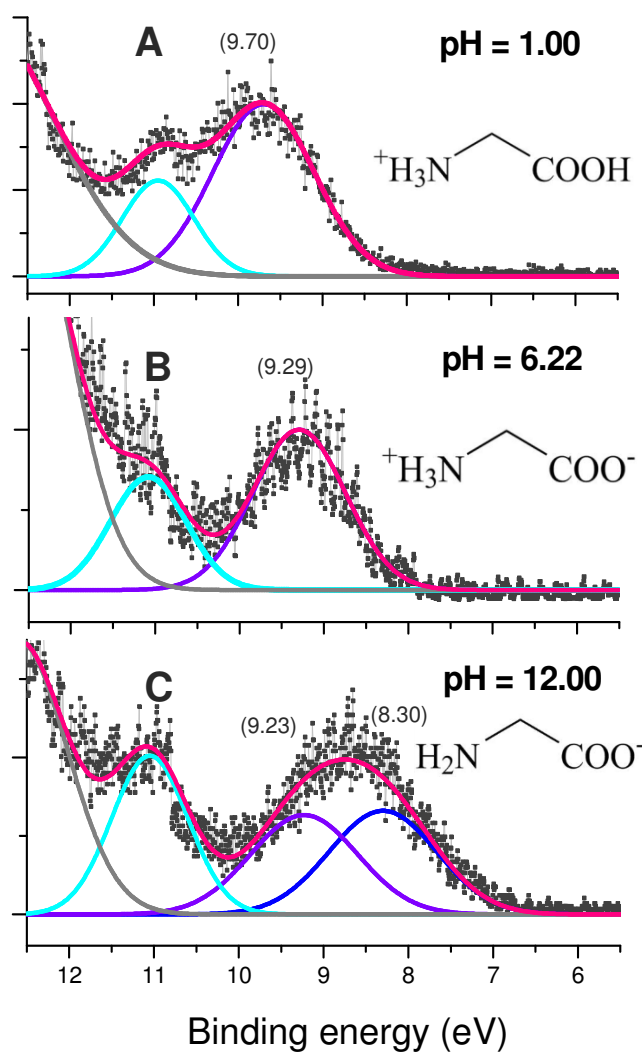

Figure S4 VUV photoelectron spectra of Gly aqueous aerosols at: A. pH =1.00, B. pH = 6.22 and C. pH = 12.00. Symbol notation: experiment, -■-; Gly n_O, violet curve; Cys n_N, blue curve; condensed water, cyan curve; gas phase water, gray curve, cumulative curve, pink curve.

A new spectral feature of lower B.E. representing the Gly n_N feature is thus included in the deconvolution (blue curve in Figure S2C), and a B.E. value of 8.30 ± 0.05 eV is obtained for Gly n_N from the optimal deconvolution.

The lowering of B.E. observed for the Gly n_O feature when transformed from the Gly^+ cation (at pH = 1.00) to the Gly zwitterion (at pH = 6.22) is likely caused by the shielding effect of the carboxylate group exerted on Gly n_O upon its deprotonation, leading to a reduced effective nuclear charge and a smaller B.E. for Gly n_O. On the other hand, the B.E. of Gly n_O does not appear to alter significantly between pH of 6.22 and 12.00, likely because the main change between these two pH conditions is mostly on the amine group and the local environment of the carboxylate group of Gly remains relatively unaffected. The spectral parameters for each spectral component, including their peak position and bandwidth obtained from the spectroscopic de-convolution are listed in Table S2.

Table S2. The parameters of each spectral feature derived from the optimized deconvolution of observed photoelectron spectra of Gly aqueous aerosols at three representative pH conditions, each corresponding to a dominating charge status.

pH value	Gly nO		Gly nN		Condensed water	
	Position /eV	Width /eV	Position /eV	Width /eV	Position /eV	Width /eV
1.00	9.70 ± 0.05	1.20	-	-	10.95 ± 0.05	0.85
6.22	9.29 ± 0.05	1.20	-	-	11.08 ± 0.05	0.85
12.00	9.23 ± 0.05	1.26	8.30 ± 0.05	1.21	11.08 ± 0.05	0.90

In comparison with the I.E. of the gas phase Gly n_O at 11.20 eV, the I.E. of Gly n_O in aqueous aerosols is measured to be 9.70 eV at pH = 1.00 and 9.29 eV at pH = 6.22, corresponding to a gas-to-liquid I.E. shift of 1.5 eV and 1.9 eV under these aqueous conditions. Similarly, a gas-to-liquid I.E. shift of 1.70 eV is found for Gly n_N in the aqueous aerosol environment, as compared with the I.E. of the gas phase Gly n_N at 10.00 eV reported by Gråsjö et al[28]. It is intriguing to note that the scales of gas-to-solution I.E. shifts for Gly is very close to the gas-to-liquid I.E. shift observed for water.[3,8,31] From our previous vibrational-resolved photoelectron spectroscopic study on the pure water aerosols, the I.E. of the (0,0,0) feature of $1b_1$ band of the condensed water was observed at 10.83 ± 0.05 eV.[8] Compared to the I.E. of the (0,0,0) feature of $1b_1$ band for the gaseous water molecule, it corresponds to a gas-to-liquid I.E. shift of 1.77 ± 0.05 eV. The origins responsible for the gas-to-liquid shift for water have been discussed extensively by Winter and coworkers.[3,31] The surface dipoles, electronic polarization and the hydrogen bond-induced molecular orbital character changes have been suggested as the major factors contributing to the gas-to-liquid shift observed for water.[3,31] From the observed scale of the gas-to-liquid I.E. shift for Gly and the chemical environmental modification experienced by Gly upon solvation, the major factors governing the gas-to-liquid shift for water appear to also play roles in contributing to the gas-to-liquid shift for Gly and other solutes under the aqueous environment.

S.6. VUV photoelectron spectra of Glu aqueous aerosols at varying pH

Glutamic acid (Glu) is one of the three constituting amino acids of GSH besides Gly and Cys. To better understand the observed GSH photoelectron spectra and the possible contributions of Glu to the electronic structures of GSH, it is essential to also have a fundamental understanding on the valence electronic properties of Glu and their possible evolutions with varying pH conditions in the same aqueous phase. Aside from being the building block of GSH, Glu is of substantial biological significance itself. Glu is prevalently distributed in brain tissues and its biochemical activity is closely associated with the neural activation, neurotransmission and brain functions.[32] In specific, Glu serves as the neurotransmitter in the fast excitatory synapses transmission via interacting with a receptor, which induces a conformational transition of the receptor to open the gated ion channels. It has been suggested that Glu is more effective in forming the ligand-operated ion channels at the physiological pH condition. However, to intrinsically understand the Glu-receptor interaction and the fast excitatory synapses transmission that Glu participates, it is critical to learn the valence electronic structures of Glu under the physiologically relevant aqueous condition.

Despite its biological significance, the studies on the electron structures of Glu are relatively scarce. Deng *et al*[33] have investigated the electronic structures of glutamate dianion (Glu^{2-}) together with the aspartate dianion (Asp^{2-}) via the low-temperature negative ion photoelectron spectroscopy, from which it was suggested that the inherent asymmetry of the amine group placement leads to different impacts on shorter (Asp) and longer (Glu) chain species. Theoretically, Meng *et al*[34] characterized the potential energy surfaces of the protonated, deprotonated and zwitterionic Glu forms in the gas phase at several different levels of theory. Due to the presence of intramolecular hydrogen bonds of gas phase Glu, different conformers

may coexist, with each conformer exhibiting its own physical properties, including the rotational constants, dipole moments, IR spectra and ionization energies[34].

Characterized by an additional carboxylic acid functional group at its side chain (denoted as γ-COOH), Glu is a highly acidic amino acid. With an isoelectric point of 3.16, Glu exists mostly in the negatively charged, deprotonated anionic form under the physiological pH condition. With three possible protonation/deprotonation sites, including the α-amino group, the α-carboxylic group and the side chain γ-carboxylic group, Glu may exist in four possible charge states at varying pH, including the protonated Glu^+, the neutral Glu zwitterion, the negatively charged Glu^- anion and Glu^{2-} dianion (see Figure 5C). To obtain the valence electronic structures of Glu and their evolutions with varying charge status, the VUV photoelectron spectra of Glu have been measured for the first time in this study in the aqueous aerosol phase at four pH conditions, including pH = 1.00 (Figure S5A), 3.16 (Figure S5B), 7.56 (Figure S5C), and 12.00 (Figure S5D). These pH conditions are chosen according to the pKa values of Glu such that each chosen pH condition can represent a dominating Glu charge species.

The experiment procedures to obtain the VUV photoelectron spectra of Glu aqueous aerosols are kept the same as those adapted for GSH aqueous aerosols, except that 0.05 M of Glu solution were sent to the constant liquid feed atomizer to generate Glu aqueous aerosols due to the smaller solubility of Glu. At pH value of 1.00, 3.16, 7.56 and 12.00, the dominating charge species are Glu^+, Glu, Glu^- and Glu^{2-}, respectively. The molecular structures of the corresponding dominating species at each specified pH are illustrated along with the photoelectron spectra in Figure S5.
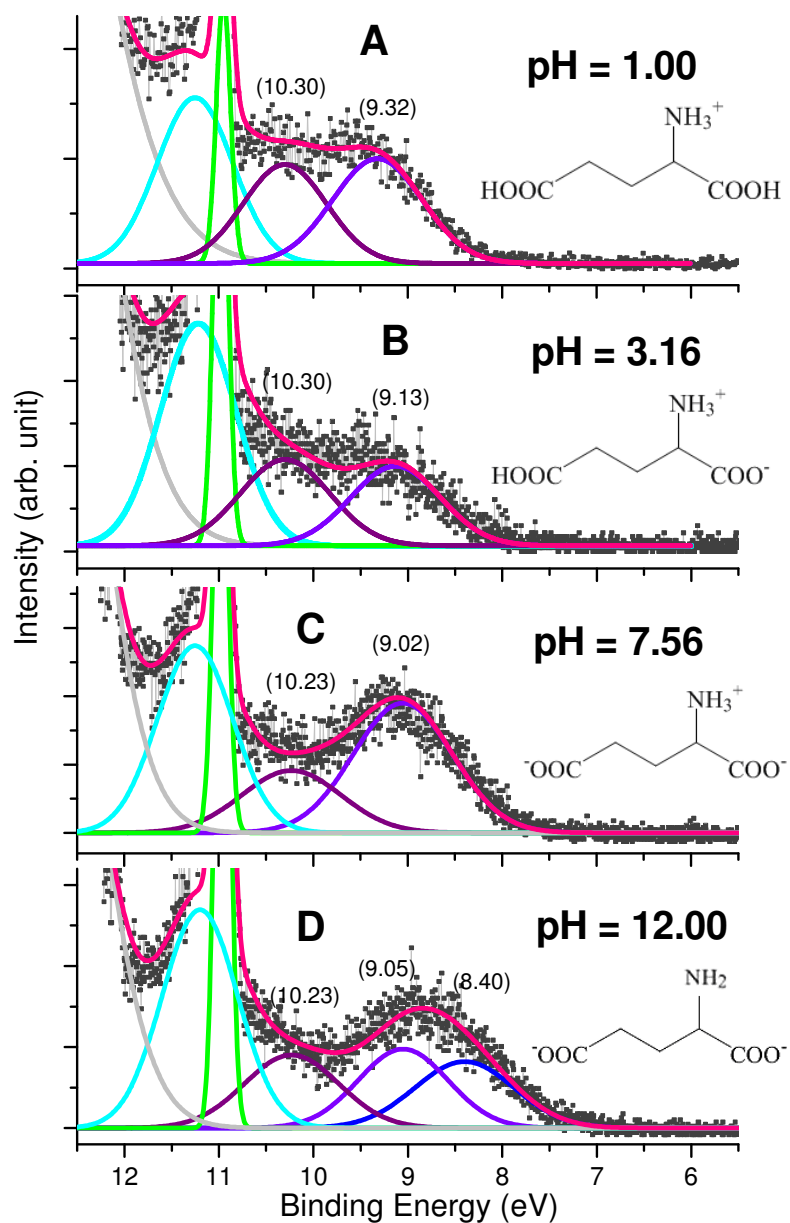
Figure S5 VUV photoelectron spectra of Glu aqueous aerosols at: A. pH =1.00, B. pH = 3.16, C. pH = 7.56 and D. pH = 12.00. Symbol: experiment, -■-; Glu n_O, violet curve; Glu n_O' (side chain), purple curve; Glu n_N, blue curve; condensed water of Glu solution, cyan curve; pure condensed water, green curve; gas phase water (only shown partially), gray curve, cumulative curve, pink curve.

The photoelectron spectral features between 11 and 7 eV (Figure S5A to D) are originated from the Glu photoelectron signals. Similar to the observed electronic evolutions for Cys[8] and Gly aqueous aerosols, the main spectral feature of Glu progressively shifts towards lower B.E. with increasing pH. To extract further insights from the observed photoelectron spectra of Glu, the spectroscopic deconvolution is also performed.

With the fully protonated Glu^+ cation as the dominating species (~94 %) at pH = 1.00, the non-bonding electrons on the oxygen of carboxyl groups are the outermost electrons to be removed upon ionization. However, due to the presence of the additional side chain carboxyl group (γ-COOH) and its considerably different local environment from the regular α-carboxyl group (α-COOH), two different spectral components have been taken into consideration in the spectral deconvolution, including the non-bonding electron on the oxygen of α-COOH (Glu n_O) and that of γ-COOH (Glu n_O'). These two carboxyl groups exhibit distinct pKa values, with the α-carboxyl group deprotonates first (pKa = 2.19), followed by the subsequent deprotonation at the γ-carboxyl group (pKa = 4.20). Though it is not immediately straightforward to distinguish the two spectral components from the Glu photoelectron spectra, hints may be obtained by tracking the evolution pattern of these two spectral features along with the corresponding local environmental change of Glu as the pH evolves.

From the optimal spectral deconvolution, the spectral feature initially centered at around B.E. of 9.32 ± 0.05 eV at pH =1 (violet curve in Figure S5A) is downshifted to 9.13 ± 0.05 eV at pH = 3.16 (violet curve in Figure S5B), and further to 9.05 ± 0.05 eV at pH = 7.56 (violet curve in Figure S5C). However, when the pH is further increased from 7.56 to 12.00, this feature does not appear to change significantly. On the other hand, the spectral feature centered at around 10.30 ± 0.05 eV at pH = 1.00 (purple curve in Figure S5A) first stays unchanged when pH is

adjusted from 1.00 to 3.16, but begins to shift to 10.23 ± 0.05 eV when pH is increased to 7.00. It remains at 10.23 ± 0.05 eV when pH is further increased to 12.00. Considering that the α-carboxyl group deprotonates prior to the γ-carboxyl group, the non-bonding electron originated from the oxygen of α-carboxyl group is expected to first experience the structural perturbation at lower pH than that of the γ-carboxyl group. Since the spectral feature of 9.32 eV at pH = 1.00 already shifted to 9.13 eV when pH is adjusted from 1.00 to 3.16, one may thus assign the feature of lower B.E. to the non-bonding electron on the oxygen of α-COOH (Glu n_O, violet curves in Figure S5) and the one of higher B.E. to that of γ-COOH (Glu n_O', purple curves in Figure S5).

Also noticeable is the main Glu feature at pH = 12.00, which appears not only shifted but also broadened when compared with the photoelectron spectra of Glu observed at other pH values. Considering that the amine group of Glu becomes deprotonated at pH = 12.00, the non-bonding electron on nitrogen of the amine group becomes subjected to ionization under this pH condition. Thus, an additional component representing this molecular orbital has been included in the spectral deconvolution of Glu photoelectron spectra (denoted as Glu n_N, blue curve in Figure S5D), and a B.E. of 8.40 ± 0.05 eV is obtained from the optimal spectral deconvolution.

Due to the lower solubility of Glu, the signals of condensed water are much more intense than that observed for GSH and Gly aqueous aerosols. Also, sharp and partially vibrational resolved condensed water feature, similar to that observed for the pure water aerosols has been observed in the Glu photoelectron spectra. This is likely so as a certain portion of condensed water in the dilute Glu aerosol may experience relatively weak solute-solvent interaction and behave almost likely the pure condensed water. In contrast, only the solute-containing condensed water feature is present in GSH, Gly and Cys aqueous aerosols, as nearly all condensed water in

these aqueous aerosols of sufficiently high concentration of solutes "senses" the presence of the solute and thus experiences considerable solute-solvent interaction.

Therefore, two types of condensed water components have been considered for deconvoluting the Glu photoelectron spectra, including a sharp and intense peak, corresponding to the pure water aerosol signals which are likely present when they evaporate from the surface of the dilute Glu aqueous aerosols (green curves in Figure S5), and a broader condensed water band (cyan curves in Figure S5) corresponding to the condensed water feature from the solute-containing aqueous aerosols. The spectral parameters derived from the optimal spectral deconvolution of Glu photoelectron spectra are listed in Table S3.

Table S3. The parameters of each spectral feature derived from the optimized deconvolution of observed photoelectron spectra of Glu aqueous aerosols at specified pH conditions.

pH	Glu nO		Glu nO'		Glu nN		Condensed water (pure)		Condensed water' (solute-containing)	
	Position /eV	Width /eV	Position /eV	Width /eV	Position /eV	Width /eV	Position /eV	Width /eV	Position /eV	Width /eV
1.00	9.32 ± 0.05	0.95	10.30 ± 0.05	0.88	-	-	10.95 ± 0.05	0.15	11.25 ± 0.05	0.80
3.16	9.13 ± 0.05	0.95	10.30 ± 0.05	0.95	-	-	10.98 ± 0.05	0.15	11.22 ± 0.05	0.80
7.56	9.05 ± 0.05	1.05	10.23 ± 0.05	1.05			10.98 ± 0.05	0.15	11.25 ± 0.05	0.80
12.00	9.05 ± 0.05	0.95	10.23 ± 0.05	1.00	8.40 ± 0.05	1.05	10.96 ± 0.05	0.15	11.20 ± 0.05	0.80

S.7. Parameters for the spectral components of Cys aqueous aerosols at varying pH

Table S4. The spectral parameters of each spectral feature derived from the optimized deconvolution of observed photoelectron spectra of Cys aqueous aerosols at four specified pH conditions, adapted from Su *et al*[8].

pH value	Cys nS		Cys nO		Cys nN		Cys nS'		Condensed water	
	Position /eV	Width /eV	Position /eV	Width /eV	Position /eV	Width /eV	Position /eV	Width /eV	Position /eV	Width /eV
1.00	8.98 ± 0.05	1.20	10.01 ± 0.05	1.00	-	-	-	-	11.10 ± 0.05	1.00
4.90	8.98 ± 0.05	0.97	9.72 ± 0.05	0.92	-	-	-	-	11.10 ± 0.05	0.95
9.00	8.57 ± 0.05	0.96	9.33 ± 0.05	0.95	10.11 ± 0.05	0.95	6.97 ± 0.05	1.30	11.10 ± 0.05	0.95
12.48	8.52 ± 0.05	0.98	9.33 ± 0.05	0.96	10.11 ± 0.05	0.95	6.97 ± 0.05	1.01	11.10 ± 0.05	0.97

SI References

(1)   Rabenstein. D.; Nuclear Magnetic-Resonance Studies of Acid-Base Chemistry of Amino Acids and Peptides. 1. Microscopic Ionization Constants of Glutathione and Methylmercury-Complexed Glutathione. *J. Am. Chem. Soc.* **1973**, *95*, 2797-2803.

(2)   Faubel, M.; Steiner, B.; Toennies, J. P. Photoelectron Spectroscopy of Liquid Water, Some Alcohols, and Pure Nonane in Free Micro Jets. *J. Chem. Phys.* **1997**, *106*, 9013-9031.

(3)   Winter, B.; Weber, R.; Widdra, W.; Dittmar, M.; Faubel, M.; Hertel, I. V. Full Valence Band Photoemission from Liquid Water Using EUV Synchrotron Radiation. *J. Phys. Chem. A* **2004**, *108*, 2625-2632.

(4)   Nishizawa, K.; Kurahashi, N.; Sekiguchi, K.; Mizuno, T.; Ogi, Y.; Horio, T.; Oura, M.; Kosugi, N.; Suzuki, T. High-Resolution Soft X-Ray Photoelectron Spectroscopy of Liquid Water. *Phys. Chem. Chem. Phys.* **2011**, *13*, 413-417.

(5)   Kurahashi, N.; Karashima, S.; Tang, Y.; Horio, T.; Abulimiti, B.; Suzuki, Y.-I.; Ogi, Y.; Oura, M.; Suzuki, T. Photoelectron Spectroscopy of Aqueous Solutions: Streaming Potentials of NaX (X = Cl, Br, and I) Solutions and Electron Binding Energies of Liquid Water and X. *J. Chem. Phys.* **2014**, *140*, No. 174506.

(6)   Henderson, M. A. The Interaction of Water with Solid Surfaces: Fundamental Aspects Revisited. *Surf. Sci. Rep.* **2002**, *46*, 1-308.

(7)   Shibaguchi, T.; Onuki, H.; Onaka, R. Electronic Structures of Water and Ice. *J. Phys. Soc. Jpn.* **1977**, *42*, 152-158.

(8)   Su, C.-C.; Yu, Y.; Chang, P.-C.; Chen, Y.-W.; Chen, I. Y.; Lee, Y.-Y.; Wang, C. C. VUV Photoelectron Spectroscopy of Cysteine Aqueous Aerosols: A Microscopic View of Its Nucleophilicity at Varying pH Conditions. *J. Phys. Chem. Lett.* **2015**, *6*, 817-823.

(9)   Faubel, M.; Schlemmer, S.; Toennies, J. P. A Molecular Beam Study of the Evaporation of Water from a Liquid Jet. *Z. Phys. D: At., Mol. Clusters* **1988**, *10*, 269-277

(10)   Smith, J. D.; Cappa, C. D.; Drisdell, W. S.; Cohen, R. C.; Saykally, R. J. Raman Thermometry Measurements of Free Evaporation from Liquid Water Droplets. *J. Am. Chem. Soc.* **2006**, *128*, 12892-12898.

(11)   Wang, X.; McMurry, P. H. Instruction Manual for the Aerodynamic Lens Calculator. *Aerosol Sci. Technol.* **2006**, *40*, 1-10.

(12)   Buck, A. L. New Equations for Computing Vapor-Pressure and Enhancement Factor. *J. Appl. Meteorol.* **1981**, *20*, 1527-1532.

(13)   Buck Research Instruments, LLC. Buck Research CR-1A User's Manual. **1996**.

(14)   Huang, J.; Bartell, L. S. Kinetics of Homogeneous Nucleation in the Freezing of Large Water Clusters. *J. Phys. Chem.* **1995**, *99*, 3924-3931.

(15)   Johari, G. P.; Hallbrucker , A.; Mayer, E. The Glass-Liquid Transition of Hyperquenched Water. *Nature* **1987**, *330*, 552-553.

(16)   Kohl, I.; Bachmann, L.; Mayer, E.; Hallbrucker, A.; Loerting, T. Water Behaviour: Glass Transition in Hyperquenched Water? *Nature* **2005**, *435*, E1-E1.

(17)   Signorell, R.; Goldmann, M.; Yoder, B. L.; Bodi, A.; Chasovskikh, E.; Lang, L.; Luckhaus, D. Nanofocusing, Shadowing, and Electron Mean Free Path in the Photoemission from Aerosol Droplets. *Chem. Phys. Lett.* **2016**, *658*, 1-6.

(18)   Goldmann, M.; Miguel-Sánchez, J.; West, A. H. C.; Yoder, B. L.; Signorell, R. Electron Mean Free Path from Angle-Dependent Photoelectron Spectroscopy of Aerosol Particles. *J. Chem. Phys.* **2015**, *142*, No. 224304.

(19)   Suzuki, Y.-I.; Nishizawa, K.; Kurahashi, N.; Suzuki, T. Effective Attenuation Length of an Electron in Liquid Water between 10 and 600 eV. *Phys. Rev. E* **2014**, *90*, No. 010302.

(20)   Thürmer, S.; Seidel, R.; Faubel, M.; Eberhardt, W.; Hemminger, J. C.; Bradforth, S. E.; Winter, B. Photoelectron Angular Distributions from Liquid Water: Effects of Electron Scattering. *Phys. Rev. Lett.* **2013**, *111*, No. 173005.

(21)   Debies, T. P.; Rabalais, J. W. Electronic-Structure of Amino-Acids and Ureas. *J. Electron Spectrosc. Relat. Phenom.* **1974**, *3*, 315-322.

(22)   Cannington, P. H.; Ham, N. S. He(I) and He(II) Photoelectron Spectra of Glycine and Related Molecules. *J. Electron. Spectrosc. Relat. Phenom.* **1983**, *32*, 139-151.

(23)   Cannington, P.; Ham, N. S. The Photoelectron Spectra of Amino-Acids: A Survey. *J. Electron. Spectrosc. Relat. Phenom.* **1979**, *15*, 79-82.

(24)   Plekan, O.; Feyer, V.; Richter, R.; Coreno, M.; de Simone, M.; Prince, K. C.; Carravetta, V. Investigation of the Amino Acids Glycine, Proline, and Methionine by Photoemission Spectroscopy. *J. Phys. Chem. A* **2007**, *111*, 10998-11005.

(25)   Gordon, M. L.; Cooper, G.; Morin, C.; Araki, T.; Turci, C. C.; Kaznatcheev, K.; Hitchcock, A. P. Inner-Shell Excitation Spectroscopy of the Peptide Bond: Comparison of the C 1s, N 1s, and O 1s Spectra of Glycine, Glycyl-Glycine, and Glycyl-Glycyl-Glycine. *J Phys Chem A* **2003**, *107*, 6144-6159.

(26)   Zubavichus, Y.; Zharnikov, M.; Schaporenko, A.; Grunze, M. NIEXAFS Study of Glycine and Glycine-Based Oligopeptides. *J. Electron. Spectrosc. Relat. Phenom.* **2004**, *134*, 25-33.

(27)   Zubavichus, Y.; Shaporenko, A.; Grunze, M.; Zharnikov, M. Innershell Absorption Spectroscopy of Amino Acids at All Relevant Absorption Edges. *J. Phys. Chem. A* **2005**, *109*, 6998-7000.

(28)   Grasjo, J.; Andersson, E.; Forsberg, J.; Duda, L.; Henke, E.; Pokapanich, W.; Bjorneholm, O.; Andersson, J.; Pietzsch, A.; Hennies, F.; Rubensson, J. E. Local Electronic Structure of Functional Groups in Glycine as Anion, Zwitterion, and Cation in Aqueous Solution. *J. Phys. Chem. B* **2009**, *113*, 16002-16006.

(29)   Ottosson, N.; Borve, K. J.; Spangberg, D.; Bergersen, H.; Saethre, L. J.; Faubel, M.; Pokapanich, W.; Ohrwall, G.; Bjorneholm, E.; Winter, B. On the Origins of Core-Electron Chemical Shifts of Small Biomolecules in Aqueous Solution: Insights from Photoemission and *ab Initio* Calculations of Glycine$_{aq}$. *J. Am. Chem. Soc.* **2011**, *133*, 3120-3130.

(30)   Wilson, K. R.; Peterka, D. S.; Jimenez-Cruz, M.; Leone, S. R.; Ahmed, M. Vuv Photoelectron Imaging of Biological Nanoparticles: Ionization Energy Determination of Nanophase Glycine and Phenylalanine-Glycine-Glycine. *Phys. Chem. Chem. Phys.* **2006**, *8*, 1884-1890.

(31)   Winter, B.; Faubel, M. Photoemission from Liquid Aqueous Solutions. *Chem. Rev.* **2006**, *106*, 1176-1211.

(32)   Krebs, H. A. Metabolism of Amino-Acids: The Synthesis of Glutamine from Glutamic Acid and Ammonia, and the Enzymic Hydrolysis of Glutamine in Animal Tissues. *Biochem. J.* **1935**, *29*, 1951-1969.

(33)   Deng, S. H. M.; Hou, G.-L.; Kong, X.-Y.; Valiev, M.; Wang, X.-B. Examining the Amine Functionalization in Dicarboxylates: Photoelectron Spectroscopy and Theoretical Studies of Aspartate and Glutamate. *J. Phys. Chem. A* **2014**, *118*, 5256-5262.

(34)   Meng, L.; Lin, Z. Comprehensive Computational Study of Gas-Phase Conformations of Neutral, Protonated and Deprotonated Glutamic Acids. *Comput. Theor. Chem.* **2011**, *976*, 42-50.